



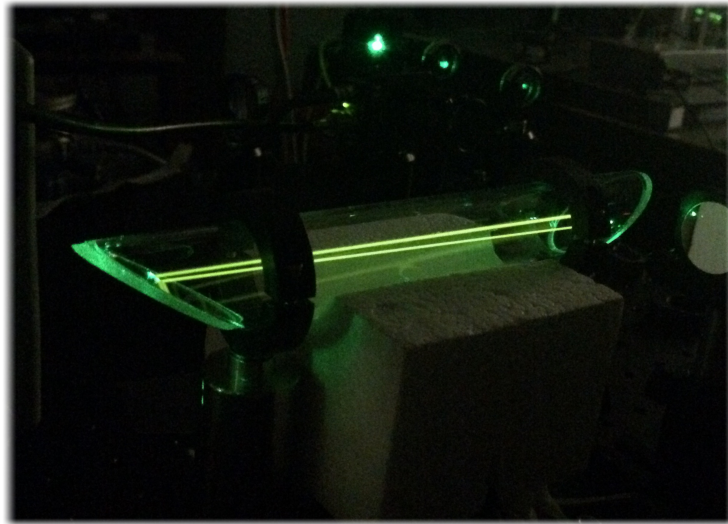
Doppler-Free Cavity Enhanced Spectroscopy of Molecular Iodine

Bachelor thesis

Sofus Laguna Kristensen

fpw119

January, 2016



Quantum Metrology Group
Niels Bohr Institute
University of Copenhagen

Supervisors:

Sigrid Skovbo Adersen

Jan Westenkær Thomsen

Resumé

Dette projekt præsenterer en eksperimentel opstilling til at udføre mættet spektroskopi på $^{127}\text{I}_2$, en lovende base for et kompakt og billigt molekylært ur. Opstillingen benytter en optisk kavitet til at forbedre interaktionslængden, hvilket giver et forøget signal-til-støj forhold. Den stærke, smalle hyperfine ro-vibrationelle overgang $P(13)43-0$ a_2 med en naturlig liniebredde på $2\pi \cdot 48$ er af interesse som en frekvens reference. Grønt lys der matcher overgangen ved 514.67 nm bliver succesfuldt genereret ved anden harmoniske generation. Dette projekt indeholder en diskussion af den underliggende teori om molekylær spektroskopi, en beskrivelse af de eksperimentelle teknikker, og en karakterisering af elementerne i den eksperimentelle opstilling. Spektroskopien af jodprøven viste den Doppler-forbrede foldning af de 21 overgange i $P(13)43-0$ manifolden, men der blev ikke observeret mættet absorption på grund af en forurening af absorptionscellen.

Abstract

This project presents an experimental setup to perform saturation spectroscopy on $^{127}\text{I}_2$, a promising base for a compact and cheap molecular clock. The setup makes use of an optical resonator to enhance the interaction length, and this provides an increased Signal-to-Noise Ratio (SNR). The strong, narrow hyperfine ro-vibrational transition $P(13)43-0$ a_2 with a natural linewidth of $2\pi \cdot 48$ kHz is of interest as a frequency reference. Green light matching the transition at 514.67 nm is successfully generated using Second Harmonic Generation (SHG). The project contains a discussion of the underlying theory of molecular spectroscopy, a description of the experimental techniques, and a characterisation of the elements in the experimental setup. The spectroscopy signal of the iodine sample revealed the Doppler-broadened convolution of the 21 transitions in the $P(13)43-0$ manifold, but no saturated absorption was observed due to a contamination of the iodine absorption cell. ¹

¹Picture on front page: Testing the iodine absorption cell using a simple double pass scheme.

Acknowledgements

First and foremost, I would like to thank my supervisors, Jan W. Thomsen and Sigrid Skovbo Ad-sersen, whose guidance was a great help in my introduction to the wonders of doing experimental laser physics.

I would also like to thank the rest of the Quantum Metrology group; Bjarke Takashi Røjle Chris-tensen, Stefan Alaric Schäffer, Martin Romme Henriksen and Stefan Mossor Rathmann, for having a friendly and helpful attitude towards a humble bachelor student.

The quality of this project has been improved dramatically by the keen eyes and minds of Marie Mørk, **Mikkel Bloch Lauritzen**, Marieke Van Beest and Peter Røhr Tunstall, who took their time to read the manuscript.

Thanks to Axel Boisen, for having a positive attitude towards all sorts of practical problems, and for fabricating electronic circuits from wiring diagrams above comprehension.

Lastly, a huge thanks to Jan Hald for letting us borrow his laser and laboratory to test our iodine cell.

Contents

Acknowledgements	iv
Contents	v
List of Figures	vi
Nomenclature	vii
1 Introduction	1
1.1 What Is a Measurement?	1
1.2 Using Quantum Metrology to Measure Gravitational Waves	1
1.3 This Project	2
2 Theory of Light and Atoms	2
2.1 Light-Matter Interaction	2
2.2 Describing Molecular Energies	3
3 Broadening Effects	5
3.1 Doppler Broadening	7
3.2 Pressure Broadening	8
3.3 Powerbroadening	8
3.4 Cavity Linewidth	8
4 Experimental Setup, Concepts and Techniques	8
4.1 Characterising Components in the Experimental Setup	9
4.1.1 Laser	9
4.1.2 Second Harmonic Generation Crystal	10
4.1.3 Optical Cavity	10
4.1.4 The Iodine Absorption Cell	13
4.1.5 Coupling of the Beam into the Cavity	13
4.2 Saturated Absorption Spectroscopy (SAS)	14
4.3 Pound-Drever-Hall (PDH) Method	16
4.4 NICE-OHMS	18
5 Spectroscopy	18
6 Conclusion	19
Bibliography	20
A Frequency Stability of Koheras Adjustik laser	21
B Vapor Pressure of Molecular Iodine as a Function of Temperature	22
C Photo of the Entire Experimental Setup	23
D Experimental Setup for Testing the Iodine Cell	24
E Scanning the Cavity Length	25

List of Figures

Introduction	1
1.1 Evolved Laser Interferometer Space Antenna (eLISA)	1
1.2 Confocal Cavity for Spectroscopy of Molecular Iodine	2
Theory of Light and Atoms	2
2.1 Four Different Absorption and Emission Processes.	3
2.2 An-harmonic Morse Potential	4
2.3 R- and P-branches in Molecular Transitions	5
Broadening Effects	5
3.1 Lorentzian Lineshape for Near Resonant Absorption	6
3.2 Illustrative Doppler-broadened Absorption Profile	7
Experimental Setup, Concepts and Techniques	8
4.1 The Experimental Setup	9
4.2 Power Output of the SHG Crystal	10
4.3 Confocal Fabry-Perot Cavity	11
4.4 Measuring the Cavity Finesse	12
4.5 Finesse Versus Temperature	14
4.6 Schematic for a Simple SAS Setup	15
4.7 Illustrative Saturated Absorption with Crossover Resonances.	15
4.8 Experimental Setup for Error Signal Generation	16
4.9 Generation of Sidebands Using an Electro-Optic Modulator.	16
4.10 Raw Data of the PDH Signal	17
Spectroscopy	18
5.1 Spectroscopy of the $P(13)43-0$ Manifold of Molecular Iodine	19
Appendix	21
A.1 Frequency Stability of Koheras Adjustik 1029 nm Laser	21
B.1 Vapor Pressure of Molecular Iodine as a Function of Temperature	22
C.1 Photo of the Entire Experimental Setup	23
D.1 Schematic of the Setup for Testing the Iodine Cell	24
D.2 Photo of the Setup for Testing the Iodine Cell	24
E.1 Experimental Setup for Scanning the Cavity length	25

Nomenclature

- BIPM Bureau International des Poids et Mesures. An intergovernmental organisation gathering and publishing metrology results.
- CEAS Cavity Enhanced Absorption Spectroscopy. A technique for enhancing the absorption signal by placing the absorption cell within an optical cavity.
- DBM Double Balanced Mixer. Produces a new beat signal based on the difference in frequency of two inputs.
- EOM Electro-Optic Modulator. Used to generate sidebands, i.e. beam components with frequencies symmetrically below and above the original carrier frequency.
- eLISA Evolved Laser Interferometer Space Antenna. A project of the European Space Agency to detect gravitational waves.
- FMS Frequency Modulation Spectroscopy. The technique of using the beating of different frequency components (sidebands and carrier frequency) to detect the dispersion or absorption associated with molecular resonances.
- FWHM Full Width Half Max. Width of the distribution, where the amplitude is half of the maximum.
- IR Infrared. Light with a frequency residing in the close to visible (700nm) to microwave regime (1mm).
- LASER Light Amplification by Stimulated Emission of Radiation. A device capable of producing coherent electromagnetic waves through amplification by stimulated emission.
- NICE-OHMS Noise-Immune Cavity-Enhanced Optical-Heterodyne Molecular-Spectroscopy. A technique used to generate a spectroscopy signal that is less sensitive to technical noise.
- PBS Polarisation Beam Splitter. Splits the beam into two separate beams with perpendicular polarisation.
- PID, PII Proportional Integral Derivative/Integral. Two types of electronic circuits used in a control system to adjust the output of a system with respect to a desired set point.
- SAS Saturated Absorption Spectroscopy. A technique used to eliminate the Doppler broadening effect in a spectroscopy signal.
- SHG Second Harmonic Generation. The process of generating light with a doubled frequency using two-photon interaction.
- SNR Signal to Noise Ratio. The strength of the signal detected versus the amplitude of the noise.

1 Introduction

1.1 What Is a Measurement?

When doing a measurement, you are comparing an unknown value to a predefined constant. This constant can conveniently be chosen as a constant of nature which does not vary in time or place, such as the speed of light in vacuum, or a certain amount of Rabi-oscillations in a quantum mechanical system. Of all measurement quantities, frequency can be measured with far the greatest precision, and many aspects of the modern society, including global trade, traffic and most sub-fields of science and technology, rely heavily on accurate and precise measurements of time and frequency [1, p. 1-7].

As of the 1. October 1983, the meter in SI-system is defined as the distance light travels in vacuum in $1/299.792.458$ s. The second was defined in 1967 as $9.192.631.770$ oscillations corresponding to a hyperfine transition of the ground state of the caesium-133 atom [2, p. 1-2]. Since the time standard of the SI-system is based on this definition, any new quantum mechanical clock capable of measuring time precisely must be compared to the existing standard before we can use it as a quantum mechanical measuring stick. The advancements within the field of precision measurements allows scientists to challenge the current limitations of experimental physics, and one of the greater modern day theories, General Relativity, is sought to be experimentally verified using laser interferometry. This will be explained in the following section.

1.2 Using Quantum Metrology to Measure Gravitational Waves

In 1916, Einstein, in his theory of General Relativity, predicted the existence of gravitational waves, which is said to be ripples in the fabric of space-time, propagating as waves at the speed of light [3]. Gravitational waves has yet to be measured directly, but some indirect evidence has been revealed. The 1993 Nobel Prize was awarded for measurements of the Hulse–Taylor binary neutron star system, which described an orbital decay matched precisely by Einstein’s predictions of energy loss by gravitational radiation [4]. In 2014, a group of astrophysicists at Harvard–Smithsonian Center for Astrophysics claimed to have observed evidence of the existence of gravitational waves, but these results have not yet led to scientific consensus among physicists due to decreasing confidence [5].

Evolved Laser Interferometer Space Antenna (eLISA) is a project of the European Space Agency (ESA). It is an attempt to provide direct evidence for the existence of gravitational waves. The concept for the eLISA-mission has three satellites arranged in a triangle orbiting the sun, each arm in the triangle approximately 1 million kilometres long [6]. By precisely measuring the length between the satellites using laser interferometry, it should be possible to observe gravitational waves squeezing and stretching the space-time as they pass by. To detect the distortion of space-time at the scale Einsteins theory predicts, one needs an ultra stable and precise frequency reference. Using an atomic oscillator offer several advantages, but the experimental setups are often big, expensive and very sensitive to physical disturbances. A promising solution is a molecular clock using the strong narrow resonances at 514.67 nm of molecular iodine. In this thesis, a compact, cheap and robust setup for a molecular iodine clock will be presented. It does not require any vacuum pumps, trapping of atoms, or atomic fountains. It possible that such a molecular clock will beat the current caesium atomic clocks in terms of both stability and accuracy [7].

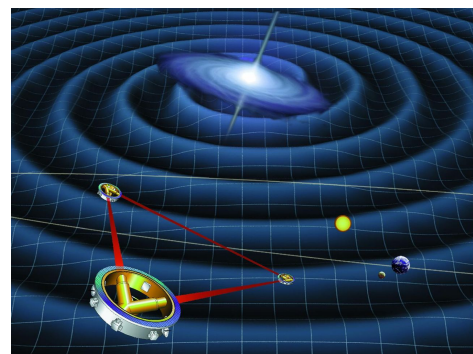


Figure 1.1: Evolved Laser Interferometer Space Antenna (eLISA). Artists impression. Picture from [6].

1.3 This Project

This project proposes an experimental setup for doing saturation spectroscopy of molecular iodine, a promising base for a stable and compact molecular clock. In this setup, the absorption cell is placed within an optical cavity (figure 1.2) for an increased interacting length, in contrast to previous projects, such as [7] or [8], using a single or double pass scheme of the iodine sample. The enhanced interaction length allows a decrease in temperature of the cell to limit pressure broadening of the resonance, while still retaining a good Signal-to-Noise Ratio (SNR) [9, p. 5]. The ro-vibrational transition $P(13)43-0 a_2$ of $^{127}\text{I}_2$ at 514.67 nm with a natural linewidth of $2\pi \cdot 48$ kHz [10] is of interest. The error signal used to lock the cavity is generated using the Pound-Drever Hall technique. Furthermore, a NICE-OHMS signal is generated. No saturated absorption signal was observed, due to a contamination of the iodine sample.

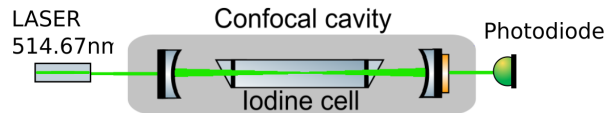


Figure 1.2: Confocal cavity for spectroscopy of molecular iodine.

The first part of this project will discuss the relevant theory regarding molecular spectroscopy. The second part will describe and review the experimental work and techniques in detail.

2 Theory of Light and Atoms

Light has long been a great mystery to physicists. After a long era of believing that light was particles moving in straight lines, "the corpuscular theory", Young's double slit experiment in 1801 seemed to confirm the theory that light was in fact waves. By shining light onto two small slits, a characteristic interference pattern could be observed on a screen behind the slits [11, p. 129-131]. However, experimental results in the early 1900's found that the energy of the light comes in discrete packets, called *quanta*, or later, photons. In the modern formulation of the theory of light and atoms, it is a known fact that particles can behave as both waves or particles. This is the so-called wave-particle duality. The wave characteristics of a particle is often described by a wave function, ψ . The square of the absolute value of this function, $|\psi|^2$, depicts the probability of finding the particle at a given point in space and time [12, p. 24-27].

2.1 Light-Matter Interaction

The energy levels in a quantum mechanical system are discrete, which means that the frequency of the light emitted or absorbed by a system must always correspond to the difference in energy between two states [13, p. 2-8]. There are four interactions with electromagnetic radiation which enables a system to change its state; stimulated emission and absorption, spontaneous emission, and non-radiative deexcitation [14]. Stimulated emission and absorption occurs when a system is exposed to electromagnetic radiation with a frequency matching the energy of the transition between the two states. Stimulated emission deexcites a system, emitting a photon identical in phase, frequency and direction to the incoming photon, thus amplifying the light. This process lays the foundation for lasers. Stimulated absorption excites the system by absorbing an incoming photon. Spontaneous emission is caused by the finite lifetime of any excited state, and happens with a certain probability within a time span [15, p. 11-13]. Non-radiative deexcitation is a process in which a system is deexcited without emitting a photon, and the excess energy is then dissipated in some other way - often in the form of quantized vibrations, known as phonons. The four processes are illustrated in figure 2.1.

The likelihood of the emitting processes depends on the transition involved. The strong transitions are those satisfying certain *selection rules*. For a simple electric dipole transition in an atom, the angular momentum quantum number l must be differing by one after absorption or emission. Therefore, all transitions involving $\Delta l = 1$ are labelled dipole-allowed [12, p. 371-374]. These transitions may nevertheless still occur when including higher-order mechanisms, such as quadrupole transitions or the magnetic dipole, but at a much lower rate than the dipole-allowed transitions.

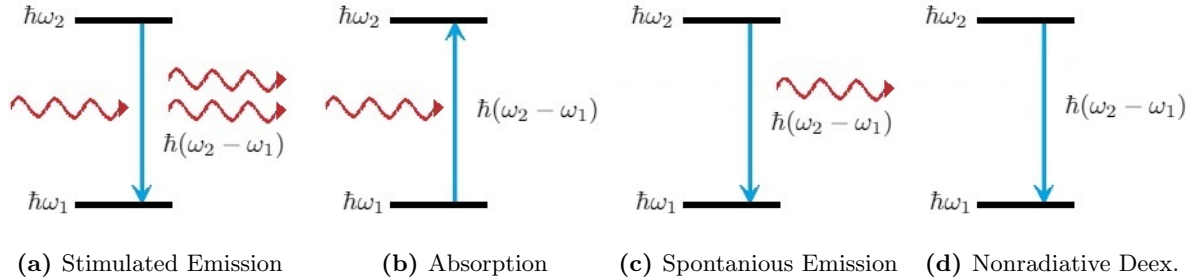


Figure 2.1: Four different absorption and emission processes. The diagrams are read as evolving in time from left to right. The red waves are photons, and the blue arrow describes the change of state.

2.2 Describing Molecular Energies

As in the case with atoms, only certain energy levels are allowed for the electrons bound to a molecule. Energy transitions in molecules caused by electron jumps often corresponds to emitting or absorbing a photon in the visible or ultraviolet region. However, unlike atoms, molecules have vibrational and rotational states, causing an additional contribution to their total energy. These energies are quantized as well, being restricted to certain values. Transitions between vibrational levels often reside in the infrared regime, whereas rotational energy levels correspond to the microwave regime [15, p. 26]. When describing molecular energy levels, using the Born-Oppenheimer approximation significantly simplifies the calculations. In this approximation, the movement of electrons are separated from the movement of the nucleus. This makes it possible to separate the wave functions, extracting the eigenvalues for the Hamiltonian separately [16]:

$$H_{tot} = H_{elec} + H_{vib} + H_{rot}. \quad (1)$$

If we consider a simple diatomic molecule, such as iodine, the binding force between the two atoms results in vibrations. Using the approximation that the binding force is linear, the potential energy function becomes:

$$V(x) = \frac{1}{2}k(x - x_0)^2, \quad (2)$$

where x is the separation between the atoms, x_0 is the stable equilibrium and k is a constant uniquely describing the potential function. The solution to this potential is a harmonic oscillator with energies given by:

$$E_n = \hbar\omega \left(n + \frac{1}{2} \right), \quad n = 0, 1, 2, \dots \quad (3)$$

However, real diatomic molecules have vibrational spectra that are described by slightly an-harmonic Morse potentials [15, p. 28-29]. By Taylor expanding the Morse potential function around the equilibrium, the vibrational energy of diatomic molecules can be written in the form

$$E_n = \hbar\omega \left[\left(n + \frac{1}{2} \right) - x_1 \left(n + \frac{1}{2} \right)^2 + x_2 \left(n + \frac{1}{2} \right)^3 + \dots \right], \quad n = 0, 1, 2, \dots \quad (4)$$

where x_i are constants determined by the an-harmonicity of the potential function. The first two, x_1 and x_2 , has been mapped for most diatomic molecules. The deviation from the harmonic oscillator increases as n becomes larger, thus decreasing the level spacing in contrast to the equidistant harmonic oscillator energy levels (figure 2.3b).

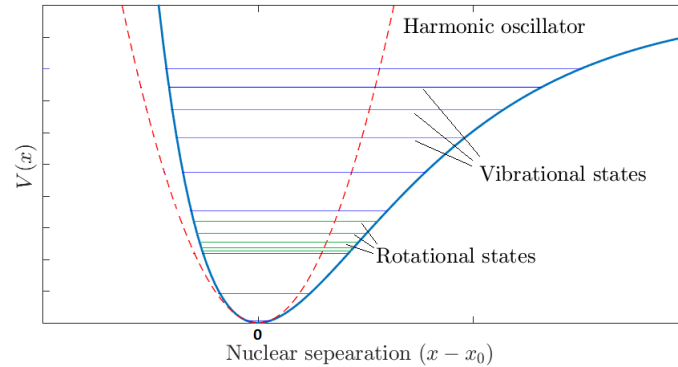


Figure 2.2: An-harmonic Morse potential as a function of the nuclear separation, for a single electronic state. The dotted red line described the harmonic oscillator approximation. The level spacing between the vibrational states decreases for higher n . The level spacing between the rotational states goes approximately as the quantum number J squared (eq. 7).

Rotations of diatomic molecules can, to first order, be described as two dumbbells with masses m_1 and m_2 rotating around their center of mass, held together by an approximately rigid massless rod. The moment of inertia for the system is:

$$I = mx_0^2, \quad (5)$$

where m is the reduced mass, and x_0 is the internuclear separation. If the angular velocity is ω_R , the angular momentum L is $I\omega_R$. The rotational energy of the system then becomes:

$$E = \frac{1}{2}I\omega_R^2 = \frac{L^2}{2I}. \quad (6)$$

Treating the system quantum mechanically, the operator L^2 yields the eigenvalues $\hbar^2 L(L+1)$ [12, p. 177]. This leads to:

$$E_{rot} = \frac{\hbar^2}{2I}J(J+1) \equiv hcBJ(J+1), \quad J = 0, 1, 2, \dots, \quad (7)$$

where B is defined as the rotational constant, and J is the rotational quantum number.

Combining the approximate electric, vibrational and rotational energies yields the total energy of the molecule:

$$E_{total} = E_e(R_0) + \hbar\omega_0 \left(n + \frac{1}{2} \right) + hcBJ(J+1), \quad (8)$$

where $E_e(R_0)$ is the electronic potential. Since the projection of J can take the values $0, \pm 1, \pm 2, \dots, \pm J$, the degeneracy of each level is $2J+1$. The level spacing of the rotational states goes approximately as J^2 . The selection rules for rotational states has $\Delta J = \pm 1$ [1, p. 124-130], and this gives rise to the so-called R- and P branches in the absorption spectrum for diatomic molecules. The R- and P branch respectively represents all the transitions where ΔJ is equal to $+1$ and -1 , and they appear symmetrically around the frequency corresponding to $\Delta J = 0$. The calculations performed however assumes that vibration and rotation are uncoupled states, but as the molecule vibrates, the moment of inertia changes, affecting the rotational energy. This decreases the rotational energy with increasing J , and breaks the apparent symmetry of the R- and P branch. It increases the energy separation for the

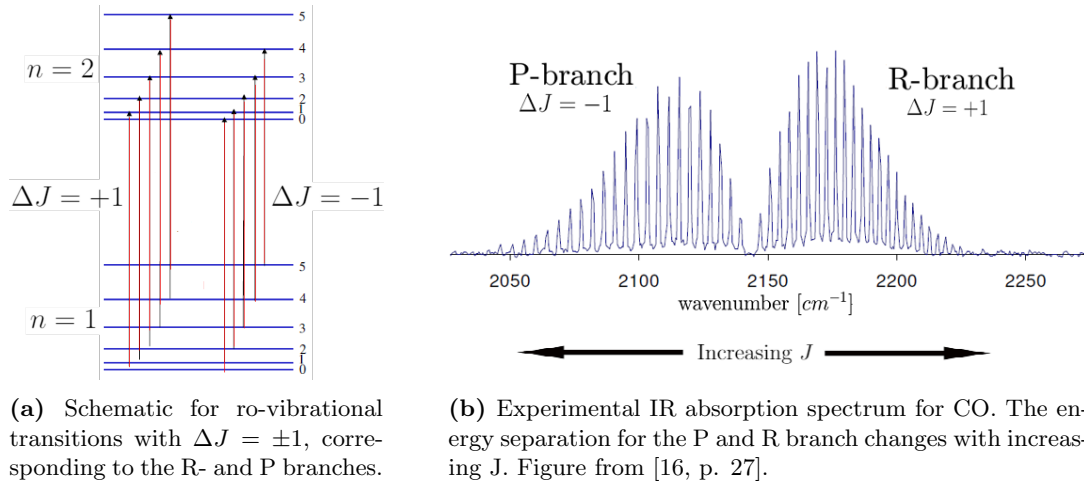


Figure 2.3: R- and P-branches in molecular transitions

P branch and decreases it for the R branch as J increases. This can be observed in figure 2.3a. The intensity of the different transitions in the branches vary due to the temperature dependent population of the different states, and the degeneracy of the states [16].

The transition of interest is $P(13)43-0 a_2$. For the rotational state, it is a transition from the 13. to the 12. state. The vibrational state changes from the ground state to the 43. level, and the electron jumps to its first excited state [8, p. 73]. This transition is further split into 21 hyperfine sublevels, due to the coupling of the molecular angular momentum and the spin of the nucleus. The a_2 component of the 514.67 nm transition is suitable for using as frequency reference in a molecular clock, due to its long lifetime and strength. The long lifetime is explained by the Frank-Condon principle, which states that the rate of a ro-vibrational transition is affected by the overlap of the wave functions for the vibrational states. The electron transition can be considered being instantaneous compared to the nuclear motion, meaning that if the nuclear position and motion is not compatible before and after the electronic transition, the transition will be very unlikely to occur [17]. If a transition is unlikely to occur, the associated energy will be very well defined, making it suitable as a frequency reference. The reason for this will be discussed in the next section.

3 Broadening Effects

In the previous chapter the possible transitions of a simple two-level atom or molecule was described. These considerations however assumed that the electromagnetic radiation absorbed or emitted is characterized by a single frequency, and that the energy levels are infinitely sharp. Neither of these conditions are satisfied in the real world. Every particle has an absorption line profile, a measure of how likely it is that the particle will absorb incoming photons as a function of the light frequency. Many mechanisms of nature contributes to the width of this absorption profile, limiting the sharpness of the transition.

Heisenberg's uncertainty principle constrains the product of the uncertainty of the energy and lifetime of a system as [12, p. 126]:

$$\Delta E \Delta t = \frac{\hbar}{2}. \quad (9)$$

This suggests that for states with short lifetimes, there will be a significant uncertainty related to

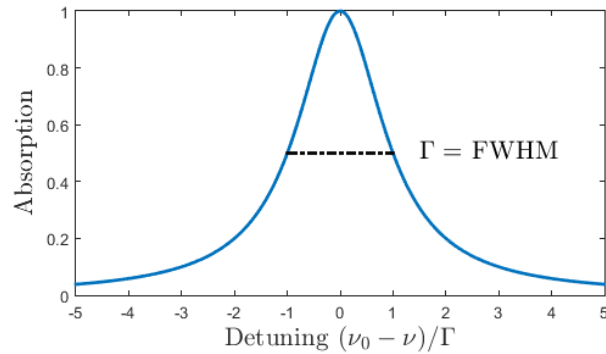


Figure 3.1: The Lorentzian lineshape $A(\nu)$, with the natural linewidth, Γ , near resonant absorption

its energy. If (9) is rewritten as:

$$\Delta E = \frac{\hbar}{2\Delta t}, \quad (10)$$

we obtain the definition for the *natural linewidth* as $\Gamma \equiv \hbar/\Delta t$. The natural linewidth is what remains when all other broadening effects can be neglected under perfect conditions. The absorption line profile for the natural linewidth is characterized by a Lorentzian line shape:

$$A(\nu) = \frac{1}{1 + \frac{(\nu_0 - \nu)^2}{\Gamma^2}}, \quad (11)$$

where ν_0 is the transition resonance frequency.

Any mechanism limiting the lifetime of a state will result in a greater uncertainty of the energy, a distortion of the energy levels. This distortion can also be interpreted mathematically as the Fourier transform of the wave packet of the state. The shorter duration of the pulse, the broader the distribution in frequency space [12, p. 125]. Thus, if state only exists for a relatively brief period, the associated energy is not well defined. In general, there are two kinds of broadening effects; inhomogeneous and homogeneous broadening effects. The inhomogeneous broadening effects affects the absorption of individual particles in an ensemble differently. An example of this is the *Doppler broadening* effect, as the Doppler shifts are velocity dependent. The homogeneous broadening effects are those equally affecting different radiating or absorbing atoms or molecules, such as the natural linewidth [18].

In the next section, the relevant broadening effects for this experiment are discussed. These effects can act alone or in combination with others. Under the assumption that each effect is independent, the observed line profile is a convolution of the line profiles of each broadening effect. The convolution of two functions is defined by:

$$(f * g)(t) = \int_{-\infty}^{\infty} f(\tau)g(\tau - t)d\tau. \quad (12)$$

A combination of a Gaussian and Lorentzian line profile yields a Voigt profile [15, p. 108-109], a common line profile in spectroscopy. An underlying assumption to the statement that the broadening effect are independent is that the mean free path of the molecules is greater than the wavelength of the transition. Otherwise, the particles may change their velocity and direction many times during emission or absorption, thus causing an average over different velocity classes, resulting in a narrowing of the linewidth. This is known as the Dicke-effect.

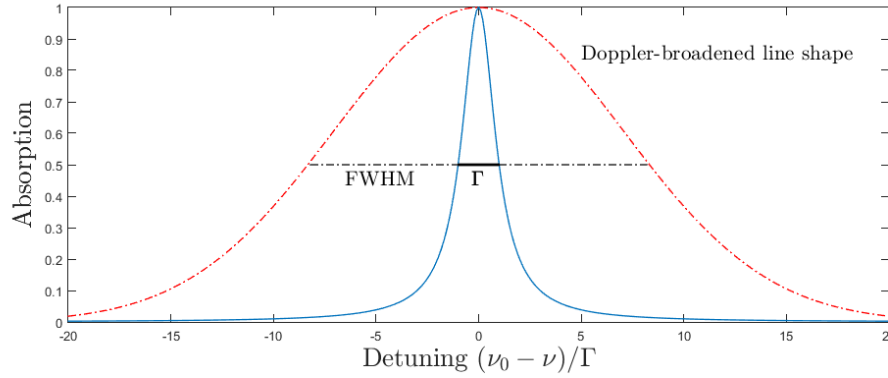


Figure 3.2: Illustrative Doppler-broadening of the absorption profile. The Doppler FWHM is much larger than the natural linewidth, Γ , of the transition.

3.1 Doppler Broadening

If an object emitting a wave is moving with a velocity relative to an observation, the observed wave will be shifted in frequency. This shift can be used to determine the velocity of the object moving, as the strength of this shift depends on the velocity. The shift in frequency is due to the Doppler-effect. Light emitted or absorbed by atoms or molecules is shifted in the same way, due to the velocity of the particles. The absorption profile of an ensemble of molecules will therefore heavily depend on the velocities of the molecules, since incoming electromagnetic waves with varying frequency will be resonant with different so-called velocity classes, when the blue- or redshifted light matches the resonance [13, p. 105-107]. For a non-relativistic thermal velocities, the Doppler-shift in frequency can be written to first order as [15, p. 105-107]:

$$\nu = \nu_0 \left(1 + \frac{v_r}{c} \right), \quad (13)$$

where v_r is the component of the velocity parallel to the wave vector of the incoming light, ν is the observed frequency, and ν_0 is the frequency in the rest frame. The probability for a molecule to have a specific velocity in a gas towards the observer is described by a Maxwellian distribution:

$$P_v(v)dv = \sqrt{\frac{m}{2\pi kT}} \cdot e^{-\frac{mv^2}{2kT}} dv. \quad (14)$$

This probability density can be expressed as a function of the frequency observed by applying the Doppler-effect,

$$P_v(\nu)d\nu = \sqrt{\frac{mc^2}{2\pi kT\nu_0^2}} \cdot e^{-\frac{mc^2(\nu-\nu_0)^2}{2kT\nu_0^2}} d\nu, \quad (15)$$

which can be recognized as a Gaussian profile, with a Full-Width Half Maximum (FWHM) of:

$$\Delta\nu_{FWHM} = \sqrt{\frac{8kT \ln(2)}{mc^2}} \nu_0. \quad (16)$$

The Doppler FWHM is often the most dominant effect on the line profile, and can place severe constraints on the precision of spectroscopic measurements figure (3.2). The effect can however be reduced by decreasing the temperature of the gas (reducing the velocity of the molecules), or eliminated by using saturation spectroscopy [19]. This technique will be explained further in section 4.2.

3.2 Pressure Broadening

In a high density gas, the molecules will constantly make soft collisions with each other. These collisions interrupts interactions with the electromagnetic field, thus shortening the characteristic time for emission processes. This results in an increased uncertainty on the energy. The mechanism depends both on the density and temperature of the gas. By decreasing the temperature of a gas, you can limit the number of collisions, and lower the uncertainty on the energy. Pressure broadening is a homogeneous broadening effect with a Lorentzian line profile [13, p. 165].

3.3 Powerbroadening

When a two-level system experiences increasingly high intensity electromagnetic radiation, with a frequency corresponding to its resonance frequency, the rate of absorption and stimulated emission will keep rising, until a point where it is much greater than the rate of spontaneous emission. This causes the population of the two states of the system to become approximately equal, effectively saturating the system. When this happens, the beam is constantly exciting and deexciting the system at almost equal rates. This leads to powerbroadening of the resonance, as the high intensity laser beam limits the lifetime of the states. The FWHM of the power broadening can be shown to be [13, p. 142-143]:

$$\Delta\nu_{FWHM} = \Gamma \sqrt{1 + \frac{I}{I_{sat}}}, \quad (17)$$

where I_{sat} , the *saturation intensity*, is the intensity required for achieving significant saturation of an absorber, and Γ is the natural line width. Eq. 17 shows that the width of the profile goes approximately as the root of the intensity. Powerbroadening is a homogenous broadening mechanism with a Lorentzian line shape.

3.4 Cavity Linewidth

When probing a molecular transition, it is desirable that the interrogating light is well-defined in frequency. However, the photons have a limited lifetime inside the cavity due to transmission of the cavity mirrors and random scattering. A long lifetime in the cavity leads to well-defined energies of the photons probing the transition. Thus, it is desirable to achieve a high Q-value (low loss per round trip) of your optical resonator. The relevant features affecting the cavity linewidth will be discussed in section 4.1.3.

4 Experimental Setup, Concepts and Techniques

This section describes the experimental setup and reviews the different techniques and concepts used for this project. The entire setup is described in figure 4.1. Following components in the experimental setup will only be mentioned, not to be characterized and examined experimentally.

- **Lenses** Used to adjust the beam size, and to collimate the beam for mode matching.
- **Hot and Cold mirrors** Hot mirrors reflects IR light, whereas cold mirrors reflects visible light.
- **EOM** Used to generate sidebands; beam components with frequencies symmetrically below and above the original carrier frequency.
- **Iris** Used to pick out a single beam when two reflections almost overlap.
- **Free-space isolator** Used to prevent reflections back into the laser.

- **Lambda plates** Used to change the polarisation of the beam. Lambda quarter plates switches the light between circularly and linear polarisation, whereas Lambda half plates changes the direction of linearly polarised light.
- **PII- and PID-controller** Electronic circuits used in a control system for stabilisation of a parameter. They calculate an error value using the difference between the output of the system and a desired setpoint.
- **Double Balanced Mixer** Produces a new signal based on the difference in frequency of the two inputs. Used to beat frequency signals.

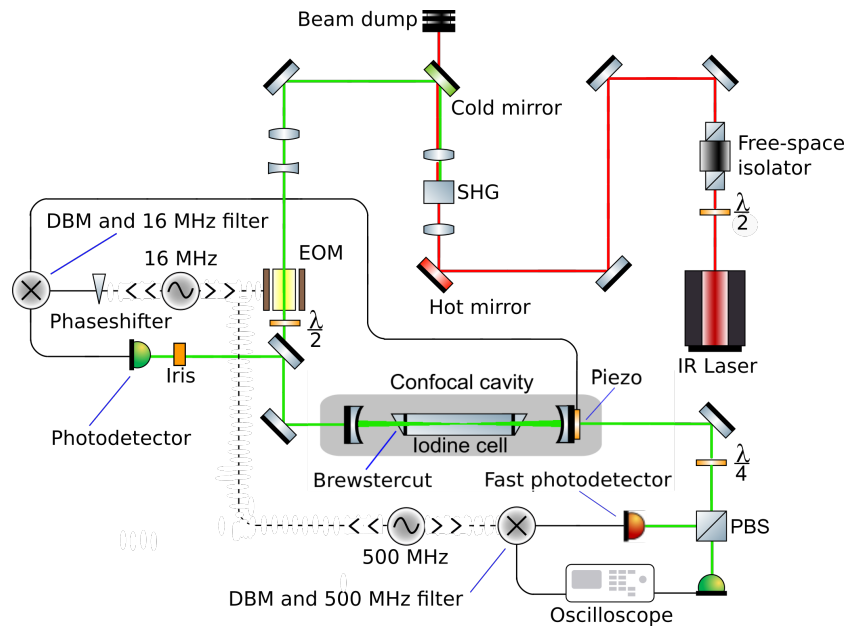


Figure 4.1: The experimental setup. Green light at 514.67 nm is generated by the SHG crystal for spectroscopy of molecular iodine.

4.1 Characterising Components in the Experimental Setup

4.1.1 Laser

The laser used in the experimental setup is a Koheras Adjustik from NKT Photonics. It is an ytterbium doped fiber laser, capable of generating light with a wavelength of 1029.34 nm with a narrow linewidth of just 3 kHz. The frequency of the laser can be tuned by either adjusting the temperature of the gain medium, or by using the built in piezo. The laser is capable of delivering 100 mW of IR power.

When the experiment failed to show signs of saturated absorption, we wanted to investigate the frequency stability of the laser. The laser was tested at the manufacturer, NKT Photonics, and the investigation revealed that the laser had been operated while a temperature stabilizing feature was enabled, making it unstable in short time spans. The investigation also did reveal a noise on the frequency of the laser with an amplitude of approximately 5 MHz. This is many magnitudes larger than the FWHM of the molecular transition we wish to investigate, which is in the kHz regime. Therefore, a mechanism to stabilise the laser, such as locking the laser to an external cavity, was desired. However, this was not realised in the time span of this project. The frequency stability of the laser with and without temperature stabilisation is shown in Appendix A.

4.1.2 Second Harmonic Generation Crystal

Second Harmonic Generation (SHG) is a process caused by a crystal's non-linearity, when the crystal lattice does not possess inversion symmetry. When an oscillating electromagnetic force is applied to the crystal lattice, the motion of the electrons will not be sinusoidal due to the an-harmonic potential. SHG doubles the frequency of a fraction of the light transmitted through the crystal by two-photon absorption. The generation of light with doubled frequency is a nonlinear process, proportional to the square of the power of the incident laser beam [13, p. 165],

$$P_{out} = \gamma \cdot P_{in}^2. \quad (18)$$

Figure 4.2 describes the power output of our SHG crystal as a function of input power and temperature. The power output of the crystal is very sensitive to temperature variations. Thus, the temperature of the crystal is stabilised to about 32.6° Celsius for maximum output. We use a Periodically Poled Potassium Titanyl Phosphate (PPKTP) non-linear crystal with a length of 15 mm for our setup.

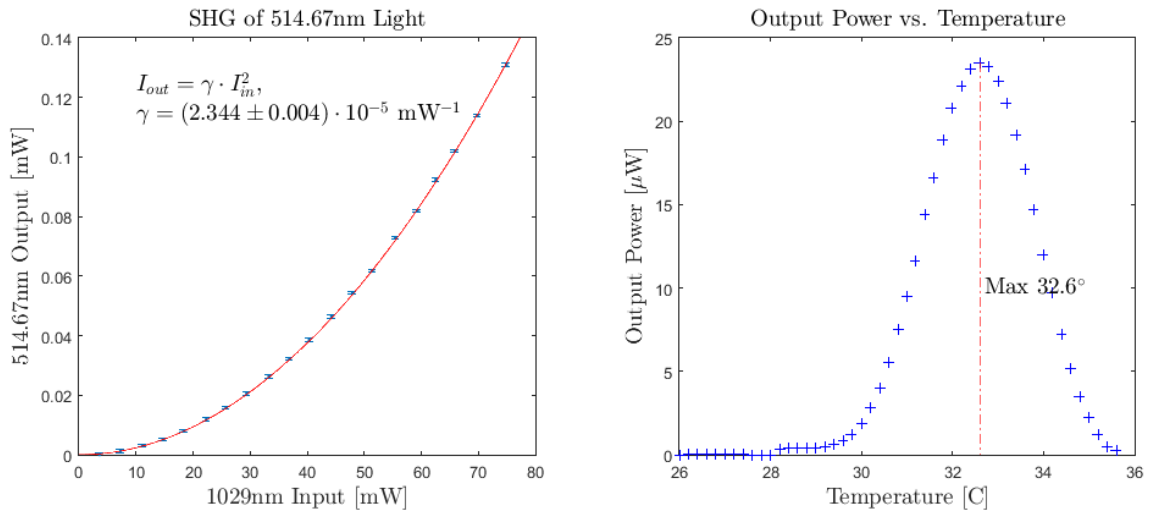


Figure 4.2: Power output of the SHG crystal as a function of input power and temperature.

4.1.3 Optical Cavity

An optical cavity is a setup of mirrors forming standing waves for light. The optical cavity supports constructive interference for certain resonance frequencies satisfying

$$L = n \frac{\lambda}{2}, \quad (19)$$

where L is the length of the cavity, n is an integer, and λ is the wavelength of the light. The allowed standing wave patterns are called modes. Frequencies causing destructive interference will be reflected of the surface of the cavity, whereas the allowed modes will enter the optical resonator [15, p. 194-198]. Optical cavities are distinguished by the focal lengths of the mirrors, and the distance between them. These are chosen so that the size of the beam in the cavity does not diverge. Our experimental setup has a Fabry-Perot cavity, a simple setup of two confocal mirrors spaced 30 cm apart, each with a 9 m radius of curvature. (figure 4.3). We will attempt to conduct saturation spectroscopy on an iodine absorption cell by placing it inside the optical resonator. This will be explained further in section 4.2.

When describing the quality of the optical oscillator, the term cavity finesse, F , is used. The cavity finesse is a unit-less measure of the loss in the cavity, and thus inversely proportional to the lifetime

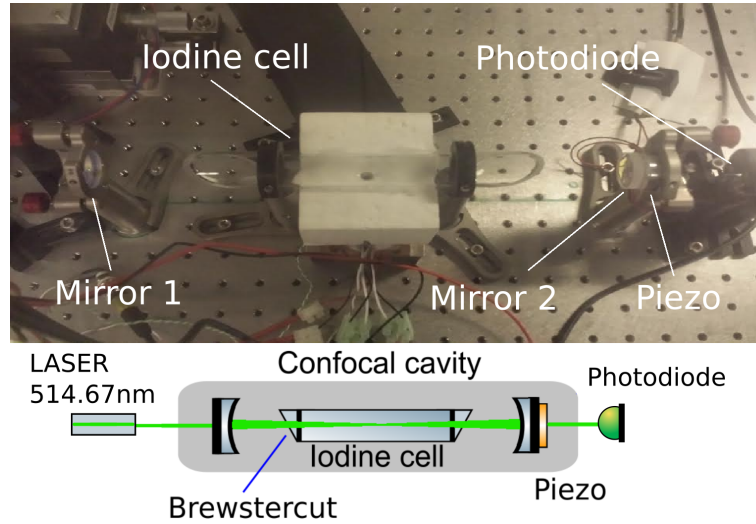


Figure 4.3: Confocal Fabry-Perot cavity around an iodine absorption cell, with piezo-electric crystal mounted behind the right mirror for cavity-locking

of a photon in the cavity. It is closely related to the Q-factor, describing the loss per period of an oscillator. The cavity enhances the effective interaction length between the laser and the absorption cell by a factor $2F/\pi$ [9, p. 10]. Factors constraining the cavity finesse includes scattering of photons in the cavity, micro roughness of the mirrors, and alignment and transmission of the cavity mirrors. The finesse of a cavity can be described theoretically by:

$$F = \frac{\pi}{2 \arcsin\left(\frac{1-\sqrt{\rho}}{2\rho^{1/4}}\right)} \approx \frac{\pi}{1-\sqrt{\rho}} \approx \frac{2\pi}{1-\rho}, \quad (20)$$

where $1-\rho$ is the loss per roundtrip [20]. The above approximation only holds for high finesse cavities with low round trip losses, for ρ close to one. A rough estimate of the highest possible finesse for the cavity, without the absorption cell, can be found by using the only well known contribution to the loss of the cavity, the transmission of the cavity mirrors, $T_{1,2} = 0.005$. This factor corresponds to a transmission of 0.5% for each time the light is reflected off a mirror.

$$F = \frac{2\pi}{Loss} = \frac{2\pi}{0.005 + 0.005} \approx 630. \quad (21)$$

This estimate is the highest possible value for the cavity finesse, limited by the transmission of the cavity mirrors.

The cavity finesse can be found experimentally as the Free Spectral Range (FSR), divided by the Full-Width Half Maximum (FWHM) of the Lorentzian of its resonance:

$$F = \frac{FSR}{FWHM}, \quad (22)$$

where the FSR is defined as

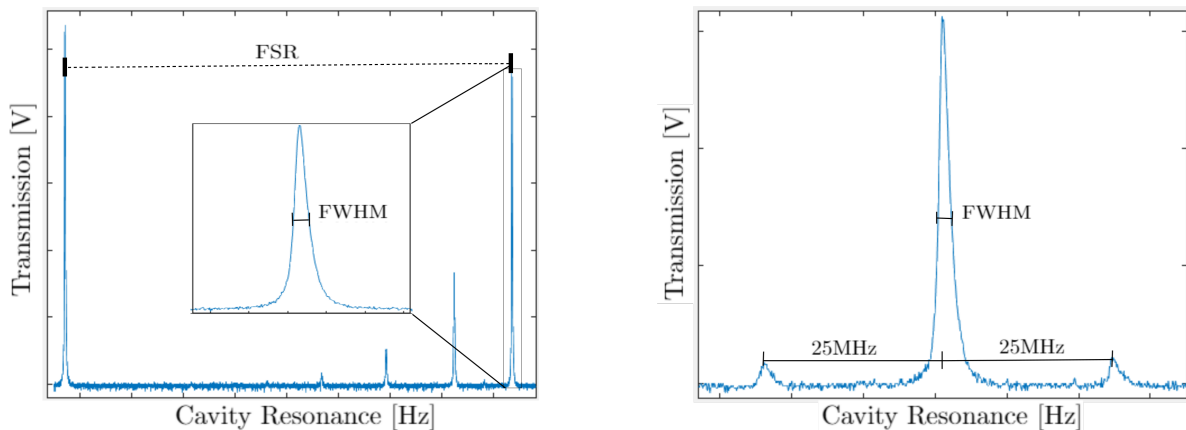
$$FSR = \frac{c}{2nL}, \quad (23)$$

L being the length of the cavity, and n the refractive index. The FSR is the difference in frequency between two successive first-order modes in the cavity. Thus, the FSR is inversely proportional to the optical path length of cavity. The FSR for our cavity is approximately 500 MHz.

The length of the cavity needs to be an integer times half the wavelength for the light to be transmitted into the cavity. To satisfy that condition, one of the cavity mirrors is glued to a piezo electric crystal, a crystal that expands when a high voltage is applied. This makes it possible to vary the length of the cavity, or stabilise it, so that the cavity constantly supports constructive interference, maximising the transmission. Stabilising the cavity (cavity locking), will be discussed in section 4.3. The finesse of the cavity can be approximated by scanning the cavity length with the piezo, and comparing the FWHM of the cavity resonance to a frequency reference present in the collected data. In this project, two different methods of measuring the finesse have been used, using either sidebands or the FSR as a reference.

The transmission through the cavity is not a direct function of frequency, but a function of the piezo position, since we vary the voltage over the cavity piezo using a triangular pulse. However, since the FWHM and the reference are measured in the same experiment, a division of the two values will yield the finesse.

Raw data for a measurement of the finesse using the FSR as a reference is depicted in figure 4.4a. Using this method, a cavity finesse of 640 was achieved with no absorption cell present, which is comparable to the theoretical approximation of 630.



(a) Measuring finesse sweeping through an entire FSR. The finesse was measured to be 640.

(b) Using sidebands as a frequency reference. A finesse of 420 was measured.

Figure 4.4: Raw data of the transmitted intensity for the cavity as a function of the cavity length. No absorption cell is present. Data from (a) and (b) are not collected from the same alignment.

However, we observed that the piezo electric crystal possesses some hysteresis, which means that the derivative of the piezos position versus time varies, potentially shifting the mutual scale of the measured values. When measuring the FSR and FWHM of the system using the FSR as a reference, one should be aware that this method only yields rough estimate of the cavity finesse. The FWHM was observed to be much smaller when close to the turning point of the piezo, which is a direct consequence of the hysteresis. To measure the cavity finesse with greater precision, you must be able to assume that the measured values are varying approximately linearly; this is only a fair assumption when the variation in position is small. Using an Electro-Optic Modulator (EOM), you can generate sidebands with a well-defined small separation frequency with respect to a carrier frequency. The separation frequency can be used as a reference by comparing it with the known FSR of the system, calculated using eq. 23. By using sidebands as a reference, the cavity finesse can be measure with greater precision, due to reduced influence of the piezo hysteresis. Figure 4.4b shows a measurement of the cavity finesse using sidebands, yielding a value of 420. The setup for scanning the cavity piezo is further clarified in Appendix E.

4.1.4 The Iodine Absorption Cell

The iodine absorption cell has Brewster cut windows, which eliminates unwanted reflexes and acts as a polarisation filter at the same time. The iodine cell decreases the finesse of the cavity, as the gas and cell windows scatters photons in random directions, thus limiting the lifetime of photons in the cavity. This effect is considerably larger when the beam is on resonance with the molecules, due to increased absorption.

To reduce collisions between the molecules (pressure broadening), the cell can be cooled down to around to -45° Celsius using a three layer peltier setup. The heat generated by the peltier elements is removed from the setup using a small wind tunnel with a fan at the far end. The tunnel limits acoustic disturbances from the fan and temperature variations through out the experimental setup. The temperature of the cell is controlled by adjusting the resistors in a Wheatstone-bridge, generating a simple error signal which is fed to a Proportional Integral Derivative (PID) controller. The cooling reduces the density of the gas in the cell, as more molecules condensate at the bottom of the cell. The multi pass scheme of the surrounding cavity compensates for the decreased absorption of the cell due to lowered density. Previous projects conducting saturation spectroscopy of molecular iodine, such as [7] or [8], either used a single or a double pass scheme of the absorption cell. In [8], the temperature of their 8 cm long absorption cell was held at -5° Celsius to yield a significant Signal-to-Noise Ratio (SNR) [8, p. 59]. In [7], they compensated for the decreased absorption at temperatures around -35° Celsius by using a 4 m long absorption cell. The Bureau International des Poids et Mesures (BIPM) based [21] on these two projects.

With the beam on resonance, we achieved a finesse of 240 at -45° Celsius. However, as we feared the number of interrogated molecules at this temperature was too low to yield a good SNR, we desired a temperature around -30° Celsius, which is still -25° Celsius colder than [8]. The finesse on resonance as a function of temperature can be described theoretically by considering the absorption by the iodine gas. The absorption depends on the vapour pressure, the length of the absorption cell, and the absorption coefficient for iodine. The expression describing vapour pressure as a function of temperature for iodine has been obtained from [8]. From this, the finesse as a function of temperature can be written as:

$$F(T) = \frac{2\pi}{T1 + T2 + 2 \cdot L_{Brew} + (1 - e^{-\alpha P(T)2L})}, \quad (24)$$

where the terms $T1$ and $T2$ describes the transmission through the cavity mirrors, $P(T)$ is the temperature dependent pressure for molecular iodine (Appendix B), α is the absorption coefficient for I_2 , and L_{Brew} is the loss due to reflections on the Brewster cut cell surfaces. L_{Brew} also includes other smaller losses, such as losses due to micro roughness of the mirrors. Figure 4.5 has the finesse as a function of temperature, with a fit of the parameters α and L_{Brew} .

4.1.5 Coupling of the Beam into the Cavity

The incident beam has to match the fundamental mode supported by the mirror configuration. This mode is governed by the distance between the cavity mirrors, as well as their radius of curvature. Thus, the cavity, and the light that is to be coupled into the cavity, must have matching mode profiles for a successful coupling. This is referred to as mode matching. Lenses have been used to adjust the size and collimate the beam prior to entering the cavity, making all the components of the beam parallel. This is to ensure that the beam oscillating in the cavity does not diverge in size [15, p. 274-275]. Mirrors are used to ensure that the beam hits the cavity mirror surface perpendicular. If the mirrors are not properly aligned, it will allow higher-order modes to reside in the cavity.

Optical power in the cavity, P_c , is built up relative to the input power, P_{in} , by constructive interference, with an increase in power proportional to the cavity finesse [8, p. 5]. We desire an intensity in the cavity which is not above the maximum saturation intensity of 40 mW/cm^2 recommended by [21]. The beam, before entering the cavity, has a maximum power of $60 \text{ } \mu\text{W}$, depending on the output power of

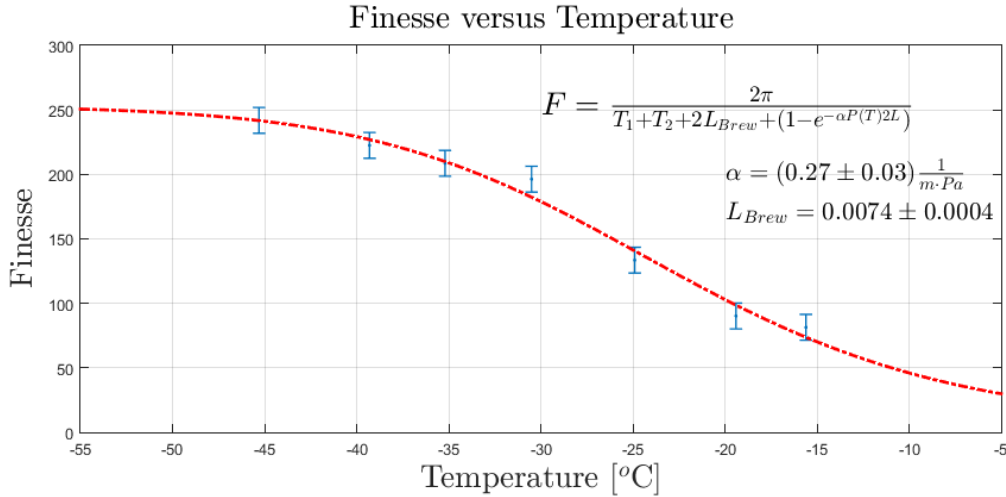


Figure 4.5: A fit of the parameters α and L_{Brew} . $T_{1,2} = 0.005$, and $L = 0.15$ m. The fit yields an estimated loss due to random scattering (mainly due to reflections on the Brewster cut cell windows) of $(0.74 \pm 0.04)\%$ per pass of the iodine cell.

the NKT laser. The SHG crystal generates more power than this, but a considerable amount (around 50%) is lost when the beam is guided through the EOM. The relationship between the incident power, P_{in} , and the accumulated power in the cavity, P_c , can be described by [8, p. 10]:

$$P_c = P_{in} \cdot T \left(\frac{1}{T + A} \right)^2, \quad (25)$$

where the T is the transmission of the mirrors, and A includes the loss due to scattering on the Brewster angled windows of the iodine cell, and the absorption of the gas,

$$A = L_{Brew} + (1 - e^{-\alpha P(T) \cdot L}). \quad (26)$$

Here, L is the length of cavity, and $P(T)$ is the pressure as a function of temperature. Therefore, the intra-cavity power is $P_c = 522.09 \mu W$ at -30° Celsius. With a beam waist of 0.4346 mm, this yields an intensity of:

$$I_c = \frac{P_c}{\pi \cdot (0.04346 \text{ cm})^2} = 87.98 \text{ mW/cm}^2. \quad (27)$$

This indicates that the intensity in the cavity suffices for the maximum saturation intensity recommended by [21]. Therefore it should be possible to conduct saturation spectroscopy.

4.2 Saturated Absorption Spectroscopy (SAS)

Saturated absorption spectroscopy is used to filter out the Doppler broadening of the absorption line profile. When scanning the laser frequency, small peaks corresponding to the resonant frequencies will appear at the bottom of the Doppler broadened transmission profile [15, p. 192-194].

The most common technique has two laser beams with the exact same frequency, preferably from the same laser, propagate through an absorption cell in precisely opposite direction. One of the lasers is considerably more intense than the other, denoted the pump beam. The counter propagating much weaker beam is referred to as the probe beam. The pump and probe beams are only interacting with molecules with a absorption profile matching the laser line profile.

When the laser is below resonance, both beams will interact with molecules blue shifting the light from the beam (molecules moving towards the origin of the respective beam). These velocity classes will not interact with the counter propagating beam, as the light from this source is red shifted. It will be appear to be far from the molecular resonance, and therefore it will not get absorbed [19, p. 1-6].

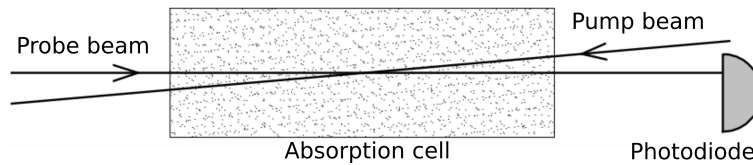


Figure 4.6: Schematic for a simple SAS setup. Figure from [19].

However, when the laser frequency is tuned to resonance, simple symmetry causes both beams to interact with same velocity class, i.e. molecules having a velocity vector perpendicular to the wave vectors of the beams. When the probe beam interrogates the molecules, it will experience less absorption, as most of the particles in the velocity class have already been excited by the pump beam. Therefore, by sweeping the frequency of our laser, we can observe a peak at the bottom of the otherwise Gaussian Doppler transmission profile of the probe beam. This is referred to as "hole burning" in the absorption. The width of this peak is defined by power broadening and the natural linewidth of the transition, and has a much smaller FWHM than the Gaussian profile. In our setup the saturation spectroscopy is done using Cavity Enhanced Absorption Spectroscopy (CEAS). By applying a multi pass scheme, the molecules are saturated by a beam which propagates through the absorption cell multiple times [13, p. 156-161].

When doing molecular spectroscopy, the Doppler FWHM for a single transition may contain many hyperfine transitions. When two or more transitions sharing the same ground state has overlapping Doppler line shapes, it will cause so-called cross over resonances. If the separation of the transitions is small compared to their Doppler width, the combined absorption profile would appear as a single Gaussian. Crossover resonances appear exactly in the middle of two real resonances due to symmetry, as the pump and probe beams are resonant with the same two opposite velocity classes (figure 4.7). The pump beam depopulates the ground state for both velocity classes, and this results in reduced absorption of the probe beam when the laser is tuned midway between the two resonant frequencies [19, p. 9-11].

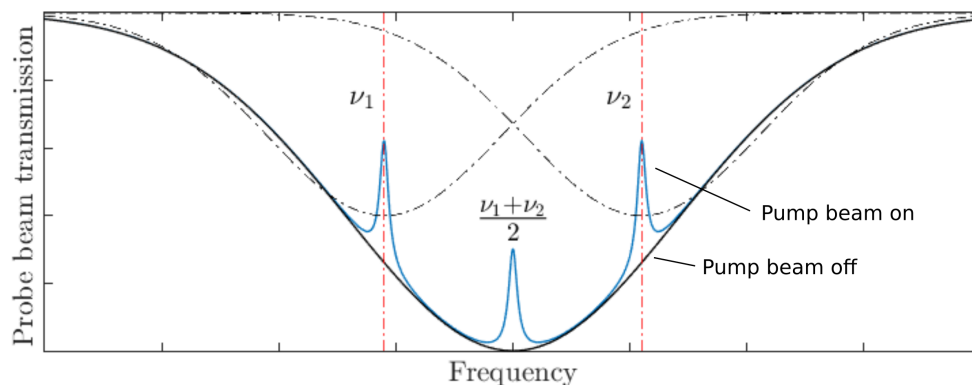


Figure 4.7: Illustrative saturated absorption with cross over resonances. The two frequencies, ν_1 and ν_2 corresponds to direct resonances, whereas $(\nu_1 - \nu_2)/2$ is a crossover resonance. The dotted lines describes the individual Doppler line profiles for the two transitions.

4.3 Pound-Drever-Hall (PDH) Method

An error signal is the difference between a system input and desired output. It is a common and powerful tool when designing a control system. In our case, we need an error signal to lock the cavity, ensuring constructive interference of the lower order longitudinal modes, by varying the length of the cavity using a piezo electric crystal. Having constructive interference in the cavity ensures that the light will be transmitted through the cavity and the absorption cell, thus making spectroscopy of our sample possible. We need the error signal to compensate for disturbances (e.g. acoustic, thermal) which may disrupt this condition. Furthermore, when scanning the relevant frequency spectrum, the length of the cavity must change accordingly in order to support constructive interference, as the length of the cavity needs to be integer times half the wavelength.

The error signal is generated using the Pound-Drever-Hall method. It is an elegant phase modulation spectroscopic method which is used to stabilise a system to an optical resonator. It utilises the fact that when a beam is reflected from the optical resonator, its amplitude and phase undergo a modulation [9, p. 45].

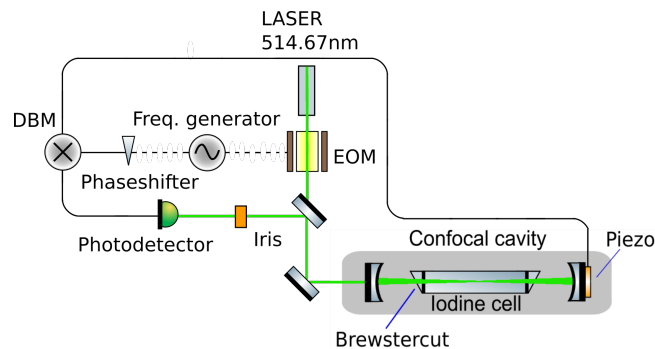


Figure 4.8: Setup for the generation of the errorsignal. The mixing with the piezo scan signal and the feeding of the PII-controller is not included.

The Pound-Drever Hall method has an incident laser beam with frequency ω modulated by an EOM with the frequency ω_m , thus creating sidebands with frequencies $(\omega - \omega_m)$ and $(\omega + \omega_m)$ (figure 4.9). The intensity of the beam reflected back from the optical resonator is measured using a fast photo detector. The photo current of the diode consists of the three fields and their component beat frequencies. A filter only allowing frequencies of ω_m is applied, such that only the beat frequencies between the sidebands and the carrier frequencies will be considered [1, p. 271-275].

The modulation frequency ω_m and the signal from the photo diode is mixed using a double-balanced mixer (DBM). Furthermore, a phase shifter is used between the modulation signal source and the DBM,

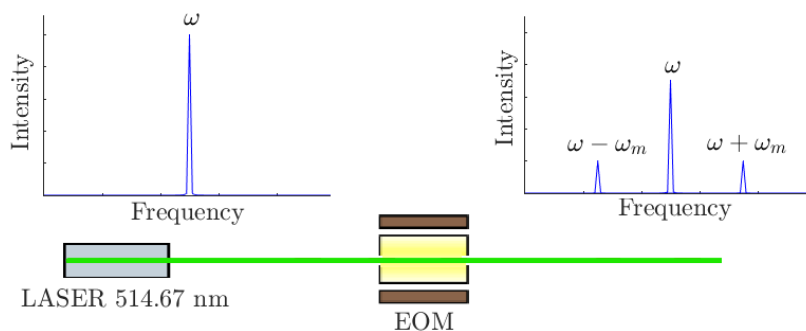


Figure 4.9: Generation of sidebands using an electro-optic modulator (EOM).

making it possible to adjust the phase relationship of the DBM inputs. When scanning the cavity piezo, at certain lengths the cavity will support constructive interference for one of the modes in the laser beam. When this happens, the resonant component of the beam will enter the cavity, affecting its phase. This means that the signal consisting of the beating of the components in the reflected beam will not destructively interfere with itself, and the generated error signal will yield a non-zero value. When the cavity is on resonance with the carrier frequency, the carrier frequency will be phase shifted 180 degrees, thus imposing symmetry and causing the signals to cancel again. This means that the error signal is zero at carrier frequency resonance, causing the desired stable fix point for our system. Furthermore, as the phase modulation of a beam around resonance is anti-symmetric, the error signal generated accounts for whether the cavity length should be increased or decreased. In the theoretical derivation of the Pound-Drever-Hall signal, a sine and cosine term appears, both containing the phase of the two signals fed to the DBM. Therefore, depending on the setting of the phase shift between the modulation signal source and the reflected beat notes, we either describe the error signal using the dispersive term [1, p. 273]:

$$D(\Delta\omega) = -4 \frac{\omega_m^2 (\Gamma/2) \Delta\omega [(\Gamma/2)^2 - \Delta\omega^2 + \omega_m^2]}{[\Delta\omega^2 + (\Gamma/2)^2][(\Delta\omega + \omega_m)^2 + (\Gamma/2)^2][(\Delta\omega - \omega_m)^2 + (\Gamma/2)^2]}, \quad (28)$$

or the absorption term:

$$A(\Delta\omega) = 4 \frac{\omega_m^2 (\Gamma/2) \Delta\omega [(\Gamma/2)^2 + \Delta\omega^2 + \omega_m^2]}{[\Delta\omega^2 + (\Gamma/2)^2][(\Delta\omega + \omega_m)^2 + (\Gamma/2)^2][(\Delta\omega - \omega_m)^2 + (\Gamma/2)^2]}, \quad (29)$$

where ω_m is the modulation frequency, and Γ is the cavity linewidth. We desire the dispersion term for the most stable and reliable operation of our cavity piezo, and thus adjust the phase relationship such that the absorption term is suppressed. The error signal generated by the Pound-Drever-Hall method is added to the triangle pulse used for scanning the cavity, and the combined signal is fed to a PII-controller. The PII-controller adjusts the voltage to the piezo in accordance with the error signal, locking our cavity to the desired mode. The schematic for the setup can be seen in figure 4.8.

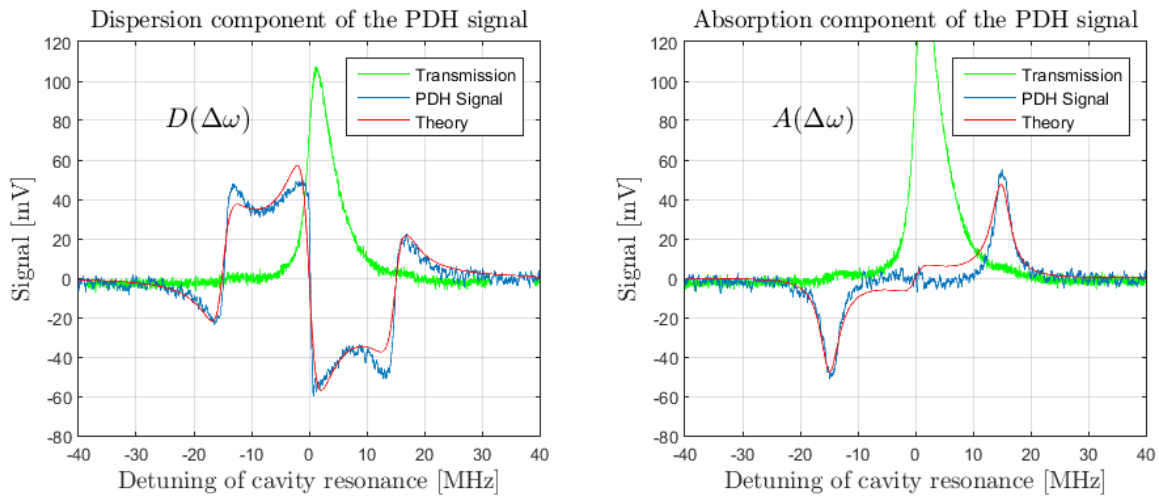


Figure 4.10: The absorption and dispersion component of the Pound-Drever Hall technique. The horizontal axis describes the detuning of the cavity resonance with respect to the carrier frequency. The green line is the signal of the light transmitted through the cavity, the blue is the raw data of the generated error signal, and the red line is the theoretical model from eq. 29 and 28 with inserted values. The frequency used for the generation of sidebands is 16 MHz, and the cavity linewidth is approximately 4 MHz. The deviation between the data and the theory is most likely a result of a slight detuning in phase between the local oscillator and the reflected beat notes.

4.4 NICE-OHMS

NICE-OHMS (Noise-Immune, Cavity-Enhanced, Optical-Heterodyne Molecular Spectroscopy) is an experimental technique that combines Frequency Modulation Spectroscopy (FMS) and CEAS. It is used to generate a spectroscopy signal that is resistant to noise from electronic parts and optical components [1, p. 302].

By feeding an EOM with a frequency equal to one FSR of the optical cavity, we generate another pair of sidebands with frequencies $\omega + \Omega$ and $\omega - \Omega$, where $\Omega = FSR$ (In our case, $FSR = 500$ MHz). The sidebands are separated from the carrier frequency with an integer times the FSR, and will therefore be transmitted through the cavity unaffected by the absorption cell. The length of the cavity is carefully chosen so that these sidebands, spaced one FSR away, will not overlap with other ro-vibrational transitions of the molecule. The carrier frequency will undergo a phase shift when on resonance with a transition. Beating the carrier frequency and the sidebands using a fast photo detector results in a signal that is at a significantly higher frequency than any common noise present in an electrical system (e.g. $1/f$ noise). The amplitude of the component oscillating at a frequency equal to the separation frequency, Ω , is picked out using a filter. This signal is mixed with the oscillator also feeding the EOM, using a DBM. This is the NICE-OHMS signal. The technique makes it possible to amplify the signal even in a high finesse cavity without drowning in technical noise [9, p. 22]. Any noise introduced by optical elements in the experimental setups will be common to the laser modes, meaning that the noise will be filtered out of the beat signal [9, p. 21-22], as these kind of disturbances do not amend the relationship of the spectral triplet.

In the experiment we made efforts to observe the phase shifts induced by the hyperfine transitions of molecular iodine, but were only able to observe the phase shift originating from the Doppler broadened absorption profile of the entire $P(13)43-0$ manifold. The NICE-OHMS signal generated when sweeping the manifold can be seen in figure 5.1.

5 Spectroscopy

Our efforts to observe saturated absorption of the iodine sample were unsuccessful. When sweeping the frequencies, we were able to observe the characteristic Doppler profile in the transmission and the associated phase shift of the carrier frequency in the NICE-OHMS signal, but the saturation of the hyperfine ro-vibrational transitions were absent in both signals. What we did observe, was the convolution of the Doppler line profiles for the 21 sharp absorption peaks in the $P(13)43-0$ branch [8, p. 74]. These have natural linewidths of magnitude ≈ 100 kHz [21], and are spread by a total of 949 MHz [8, p. 3-4]. The natural linewidth for each transition is masked by their Doppler FWHM of approximately 404 MHz at -30° degrees Celsius. Spectroscopy was attempted at approximately -30 degrees Celsius, with the power output of the NkT laser at 59 mW, 45 mW and 35 mW. The laser was scanned in frequency by feeding the laser piezo with a triangular pulse. The amplitude of this signal determines the range of the frequency sweep, and by lowering the amplitude, it was possible to zoom in on a specific part of the absorption profile. The generated NICE-OHMS signal and the transmission through the cavity for the 59 mW measurement are depicted in figure 5.1. Following the failed attempts of observing saturated absorption, the iodine absorption cell was tested at DFM (Danish Fundamental Metrology), with the aid of Jan Hald. A simple setup with a two pass scheme (Appendix D) was adapted to compare our iodine absorption cell to a reference. This comparison confirmed our suspicion towards a contamination of our iodine sample. While the iodine cell was returned to its manufacturer for refilling and resealing, we tried to obtain a saturated spectroscopy signal using another iodine cell, kindly borrowed from Jan Hald. This cell had Brewster angled windows as well, but was considerably shorter (around 70mm). Attempts to align the cavity with this new absorption cell yielded a maximum finesse of 50, which, combined with the shorter sample of iodine gas, resulted in an insufficient interaction length to gain a saturated absorption signal.

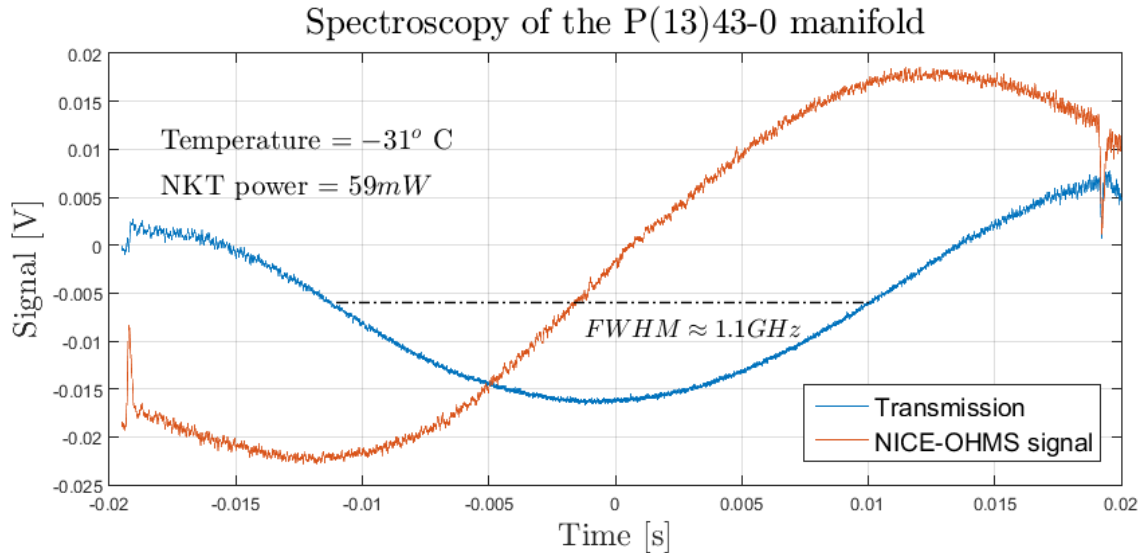


Figure 5.1: Spectroscopy of the $P(13)43-0$ manifold of molecular iodine. No saturated absorption was observed.

6 Conclusion

In the first section, the project was motivated, and the goal for project was described; successful saturation spectroscopy of the hyperfine $P(13)43-0$ a_2 transition of molecular iodine, making use of an optical resonator to enhance interaction length and thereby increase the SNR. This was in contrast to previous projects, using a single or a double pass scheme to describe the same molecular manifold. Furthermore, the project presented the relevant physics of molecular spectroscopy, gave an explanation for why the specific molecular transition is of interest as a frequency reference, and gave an overview of the relevant effects increasing the linewidth of a resonance. The experimental setup for performing saturation spectroscopy was presented. Different experimental techniques for measuring cavity finesse and for generating spectroscopy and error signals was described, and a characterisation of the different components of the setup was given. Lastly, the attempt to conduct saturation spectroscopy on the iodine absorption cell was described.

In the experimental setup, green light at 514.67 nm was generated using SHG, and $60 \mu\text{W}$ of power reached the cavity at maximum NKT laser power. This resulted in a total intra-cavity intensity of 87.98 mW/cm^2 , which suffices for the maximum of 40 mW/cm^2 recommended by the BIPM. The finesse of the optical cavity was measured to be 200 at -30° Celsius. An error signal for locking the cavity, ensuring constructive interference, was successfully generated using the Pound-Drever-Hall method. Furthermore, a NICE-OHMS signal was generated for noise-reduced spectroscopy. The transmission through the cavity and the NICE-OHMS signal yielded no trace of saturated absorption, due to a contamination of the iodine cell, which was confirmed at DFM.

The experimental setup may be improved by applying a stabilising mechanism for the laser, such as an external optical cavity fed with a fraction of the IR light. We observed and measured a significant drift in the laser frequency in short time spans, but due to the contamination of the iodine cell, we were unable to conclude whether this would hinder our attempts to observe saturation of the gas sample. The prospects for this project are still promising, but the work towards a cheap, robust and compact molecular clock has been postponed till the absorption cell is returned.

Bibliography

- [1] F. Riehle. *Frequency Standards: Basics and Applications*. Wiley, 2006. ISBN: 9783527605958. URL: <https://books.google.dk/books?id=q9AKk3smIJwC>.
- [2] Christoffer Østfeldt. *Yb3+ based Fiber Amplifier for 514 nm Iodine Spectroscopy*. The Niels Bohr Institute. 2015.
- [3] Albert Einstein. *Einige anschauliche Überlegungen aus dem Gebiete der Relativitätstheorie*. Preussische Akademie der Wissenschaften, Sitzungsberichte, 1916 (part 1), 688–696.
- [4] LIGO Caltech. *What are gravitational waves?* URL: [https://ligo.caltech.edu/page/what-are-gw/\(26-12-2015\)](https://ligo.caltech.edu/page/what-are-gw/(26-12-2015)).
- [5] Ron Cowen. *Gravitational waves discovery now officially dead*. URL: [http://www.nature.com/news/gravitational-waves-discovery-now-officially-dead-1.16830/\(26-12-2015\)](http://www.nature.com/news/gravitational-waves-discovery-now-officially-dead-1.16830/(26-12-2015)).
- [6] ESA. *eLISA Gravitational Wave Observatory*. URL: [https://www.elisascience.org/\(26-12-2015\)](https://www.elisascience.org/(26-12-2015)).
- [7] A. Goncharov. *Absolute frequency measurement of the iodine-stabilized Ar+ laser at 514.6 nm using a femtosecond optical frequency comb*. Springer-Verlag 2004. 7 April 2004.
- [8] Lisheng Chen. *High-Precision Spectroscopy of Molecular Iodine: From Optical Frequency Standards to Global Descriptions of Hyperfine Interactions and Associated Electronic Structure*. University of Colorado. 2005.
- [9] Theresa W. Lynn Jun Ye. *APPLICATIONS OF OPTICAL CAVITIES IN MODERN ATOMIC, MOLECULAR, AND OPTICAL PHYSICS*. Elsevier Science. 2003.
- [10] B. Decomps C. J. Borde G. Carny. *Measurement of the recoil shift of saturation resonances of $^{127}\text{I}_2$ at 514.5\AA : A test of accuracy for high-resolution saturation spectroscopy*. Laboratoire de Physique des Lasers, Université Paris-Nord. May 1978.
- [11] Jan W. Thomsen. *A first course in Optics*. The Niels Bohr Institute. 2010.
- [12] D.J. Griffiths. *Introduction to Quantum Mechanics*. Pearson international edition. Pearson Prentice Hall, 2005. ISBN: 9780131118928. URL: <https://books.google.dk/books?id=-BsvAQAATAAJ>.
- [13] C.J. Foot. *Atomic Physics*. Oxford Master Series in Physics. OUP Oxford, 2004. ISBN: 9780191037078. URL: <https://books.google.dk/books?id=yf6BAWAAQBAJ>.
- [14] Albert Einstein. *Strahlungs-Emission und Absorption nach der Quantentheorie*. Deutsche Physikalische Gesellschaft. 1916.
- [15] P.W. Milonni and J.H. Eberly. *Laser Physics*. Wiley, 2010. ISBN: 9780470409701. URL: <https://books.google.dk/books?id=f7g0Mx5RR3cC>.
- [16] Jan W. Thomsen. *MOLECULES*. The Niels Bohr Institute. 2010.
- [17] Edward U. Condon. *Nuclear Motions Associated with Electron Transitions in Diatomic Molecules*. Palmer Physical Laboratory, Princeton University. 1928.
- [18] RP Photonics Consulting GmbH. *Homogeneous Broadening*. URL: [https://www.rp-photonics.com/homogeneous_broadening.html\(17-01-2015\)](https://www.rp-photonics.com/homogeneous_broadening.html(17-01-2015)).
- [19] University of Florida — Department of Physics PHY4803L — Advanced Physics Laboratory. *Saturated Absorption Spectroscopy*. University of Florida. 2014.
- [20] RP Photonics Consulting GmbH. *Finesse*. URL: [https://www.rp-photonics.com/finesse.html\(26-12-2015\)](https://www.rp-photonics.com/finesse.html(26-12-2015)).
- [21] Bureau International des Poids et Mesures BIPM. *Iodine $\lambda \approx 515\text{ nm}$* . 2005.

Appendixes

A Frequency Stability of Koheras Adjustik laser

The laser was tested at NKT photonics. A temperature compensation mechanism was found to be enabled. The effect of this is to prevent frequency drift over large time spans, but this also caused the laser to make small jumps in frequency to compensate. After the laser was returned with disabled temperature stabilisation, we experienced less jitter.

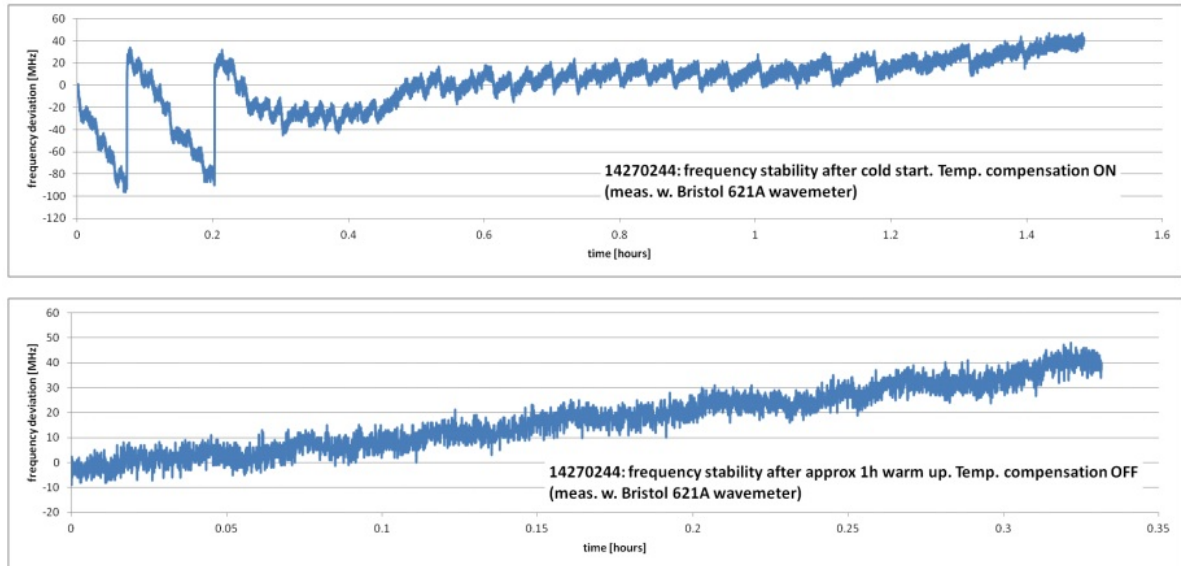


Figure A.1: Frequency stability of Koheras Adjustik 1029 nm laser.

B Vapor Pressure of Molecular Iodine as a Function of Temperature

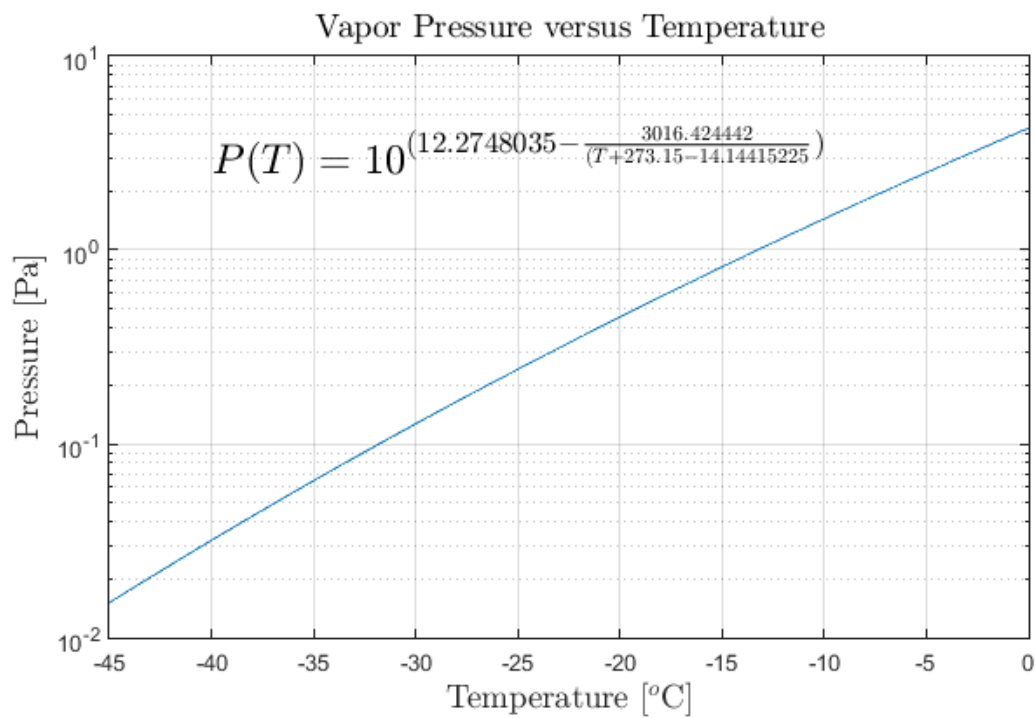


Figure B.1: Vapor pressure of molecular iodine as a function of temperature, used to predict the loss in the cavity due to absorption. The expression has been obtained from extracting reported values for temperature versus pressure from [8].

C Photo of the Entire Experimental Setup

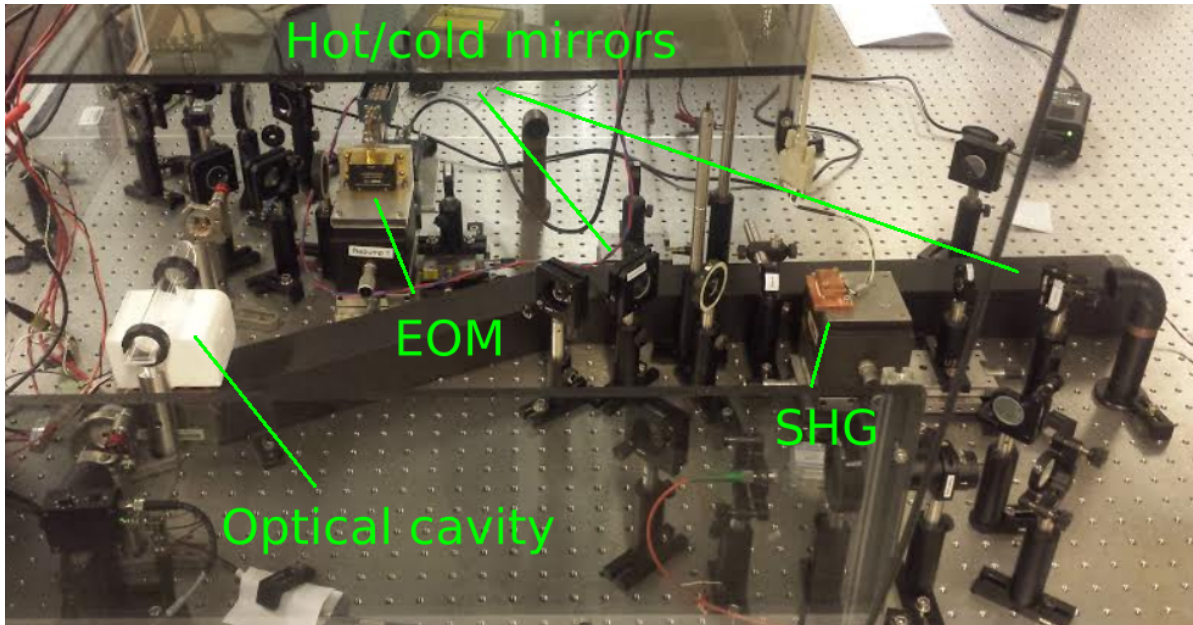


Figure C.1: Photo of the entire experimental setup in its early stages. The components for generating the Pound-Drever-Hall error signal and the NICE-OHMS spectroscopy signal has not yet been added to the setup.

D Experimental Setup for Testing the Iodine Cell

When testing the cell at Danish Fundamental Metrology (DFM), we used a considerably more intense laser at 532 nm and a two pass scheme of the absorption cell. The laser was tuned across the $R(56)32-0$ manifold. The comparison between our absorption cell and a borrowed reference cell confirmed our suspicion towards a contamination of the cell.

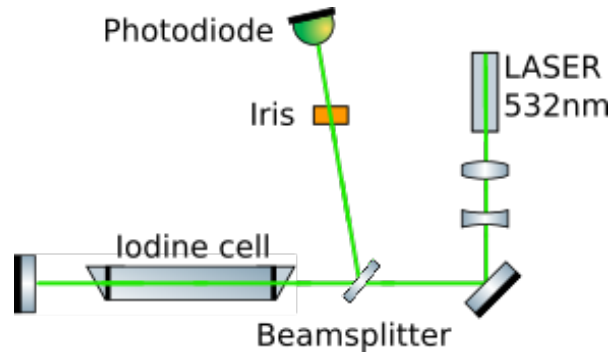


Figure D.1: Schematic of the experimental setup for testing the iodine cell.

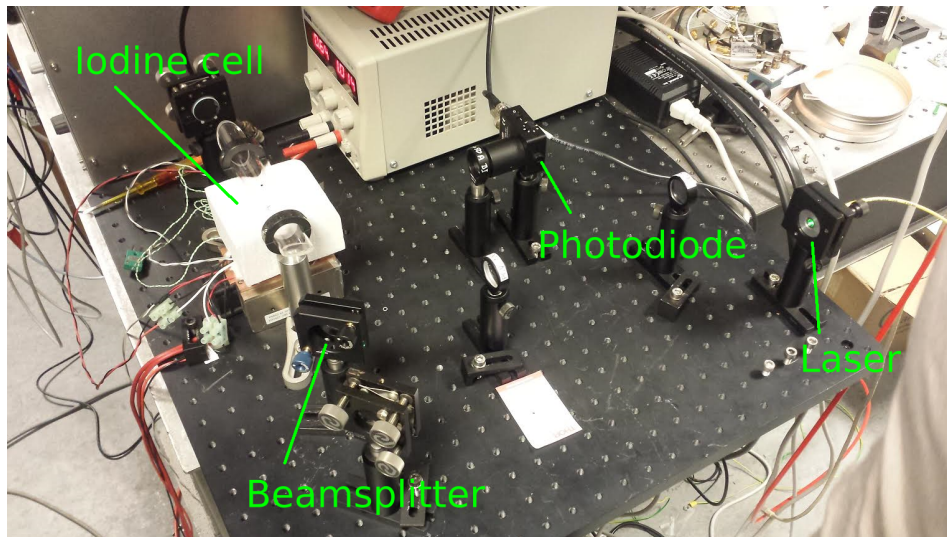


Figure D.2: Photo of the components of the setup for testing the iodine cell. The setup is not yet finished.

E Scanning the Cavity Length

Scanning the length of the cavity enabled us to estimate the cavity finesse. The amplified amplitude of the triangle pulse determines the range of the scan. The DC offset of the amplifier can be adjusted to ensure that two successive first-order modes in the cavity is visible within the range of the scan, when using the FSR as a reference for the finesse measurement.

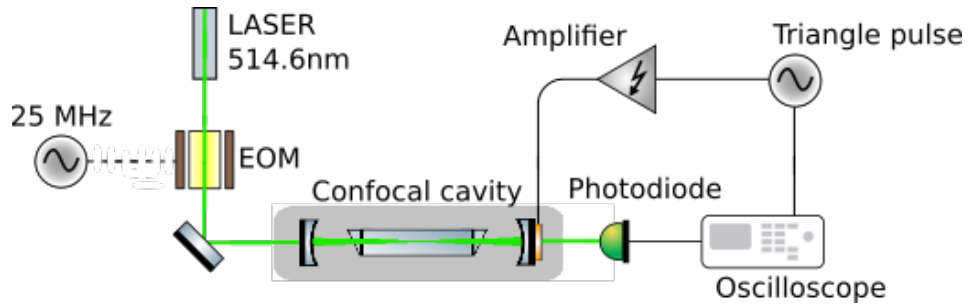


Figure E.1: Schematic of the experimental setup scanning the cavity length to determine the finesse.